Molecular Cell, Vol. 13, 497–510, February 27, 2004, Copyright ©2004 by Cell Press

Control of Actin Turnover by a *Salmonella* Invasion Protein

Emma J. McGhie, Richard D. Hayward, and Vassilis Koronakis*
Department of Pathology
University of Cambridge
Tennis Court Road
Cambridge CB2 1QP
United Kingdom

Summary

***Salmonella* force their way into nonphagocytic host intestinal cells to initiate infection. Uptake is triggered by delivery into the target cell of bacterial effector proteins that stimulate cytoskeletal rearrangements and membrane ruffling. The *Salmonella* invasion protein A (SipA) effector is an actin binding protein that enhances uptake efficiency by promoting actin polymerization. SipA-bound actin filaments (F-actin) are also resistant to artificial disassembly in vitro. Using biochemical assays of actin dynamics and actin-based motility models, we demonstrate that SipA directly arrests cellular mechanisms of actin turnover. SipA inhibits ADF/cofilin-directed depolymerization both by preventing binding of ADF and cofilin and by displacing them from F-actin. SipA also protects F-actin from gelsolin-directed severing and reanneals gelsolin-severed F-actin fragments. These data suggest that SipA focuses host cytoskeletal reorganization by locally inhibiting both ADF/cofilin- and gelsolin-directed actin disassembly, while simultaneously stimulating pathogen-induced actin polymerization.**

Introduction

Eukaryotic cells rapidly alter their shape to engulf large particles. This requires orchestrated remodeling of the actin cytoskeleton in response to external stimuli. Bacterial pathogens mimic such events to promote their internalization, survival, and dissemination by deploying virulence proteins that manipulate host cell actin dynamics. Study of these bacterial proteins not only is revealing the molecular basis of disease but is also illuminating fundamental cellular processes (Gruenheid and Finlay, 2003).

An essential stage in *Salmonella* pathogenesis is bacterial entry into nonphagocytic intestinal epithelial cells. *Salmonella* force their own uptake by inducing actin-rich filopodial and lamellipodial cell surface protrusions that envelop the bacteria and drive their internalization into a membrane-bound vacuole (Finlay and Falkow, 1997). These dramatic cytoskeletal rearrangements are triggered rapidly by the coordinated action of five *Salmonella* effectors that are delivered into the host cell (Hayward and Koronakis, 2002). The bacterial guanine nucleotide exchange factor (GEF) mimic SopE, or its homolog SopE2, together with the inositol polyphosphatase SopB activates the small cellular GTPases Cdc42 and Rac-1, triggering both actin polymerization and nuclear responses. This Cdc42/Rac-1-dependent signaling is subsequently antagonized by a third *Salmonella* effector SptP, which acts as a GTPase activating protein (GAP) (Galán and Zhou, 2000).

Salmonella also delivers two actin binding proteins (ABPs), SipC and SipA, which share no primary sequence similarity to each other or any known eukaryotic ABP. SipC is essential for cell entry (Kaniga et al., 1995) and inserts into the host plasma membrane during infection (Scherer et al., 2000). Distinct C- and N-terminal SipC domains directly nucleate actin polymerization and bundle F-actin, respectively, in vitro and induce cytoskeletal rearrangements when introduced into cultured cells (McGhie et al., 2001; Hayward and Koronakis, 1999). Both these SipC activities are stimulated by SipA, suggesting that the two *Salmonella* ABPs are likely to functionally cooperate in vivo (McGhie et al., 2001). However, unlike SipC, SipA is not essential for entry but enhances its efficiency. *Salmonella* strains lacking *sipA* induce diffuse rather than the localized actin reorganization and membrane ruffling characteristic of wild-type bacteria (Zhou et al., 1999a), although these mutants deliver all the actin polymerization-stimulating effectors into target cells. SipA localizes to cortical actin assembly zones when expressed in both mammalian cells and yeast (Higashide et al., 2002; Lesser and Miller, 2001) and binds F-actin when introduced into semipermeabilized cultured mammalian cells (McGhie et al., 2001). Biochemical characterization of SipA showed it to bind F-actin and prevent filament depolymerization in vitro (Zhou et al., 1999a; McGhie et al., 2001). SipA also promotes filament assembly by lowering the critical G-actin concentration required for polymerization (Zhou et al., 1999a; Galkin et al., 2002) and enhances F-actin bundling by host fimbrin (Zhou et al., 1999b) and bacterial ABP SipC (McGhie et al., 2001). These activities are retained by a SipA C-terminal 226 residue fragment, which also functions when fused to glutathione S-transferase (GST) (Zhou et al., 1999a, 1999b). This minimal fragment is elongated (Mitra et al., 2000) and has been proposed to span four actin monomers, connecting two protomers on opposing long-pitch helical strands, a binding mode similar to that of the eukaryotic ABP nebulin (Galkin et al., 2002).

Intracellular pathogens also utilize virulence proteins on their surface to subvert Cdc42-dependent signaling pathways, driving actin-based bacterial motility in the host cytosol. *Listeria* ActA, a eukaryotic WASP/Scar homolog, binds and directly stimulates the Arp2/3 complex (Welch et al., 1998), whereas *Shigella* IcsA mimics Cdc42-dependent N-WASP activation (Egile et al., 1999). Both these effectors stimulate continuous polarized actin assembly at the bacterial surface, leading to actin "comet tail" formation (Frischknecht and Way, 2001). Analogous structures can be generated by lipid vesicles enriched in phosphatidylinositol-4,5-bisphosphate (PIP2) that recruit Cdc42 (Ma et al., 1998). Due to their strikingly similar organization and protein comple-

*Correspondence: vk103@mole.bio.cam.ac.uk

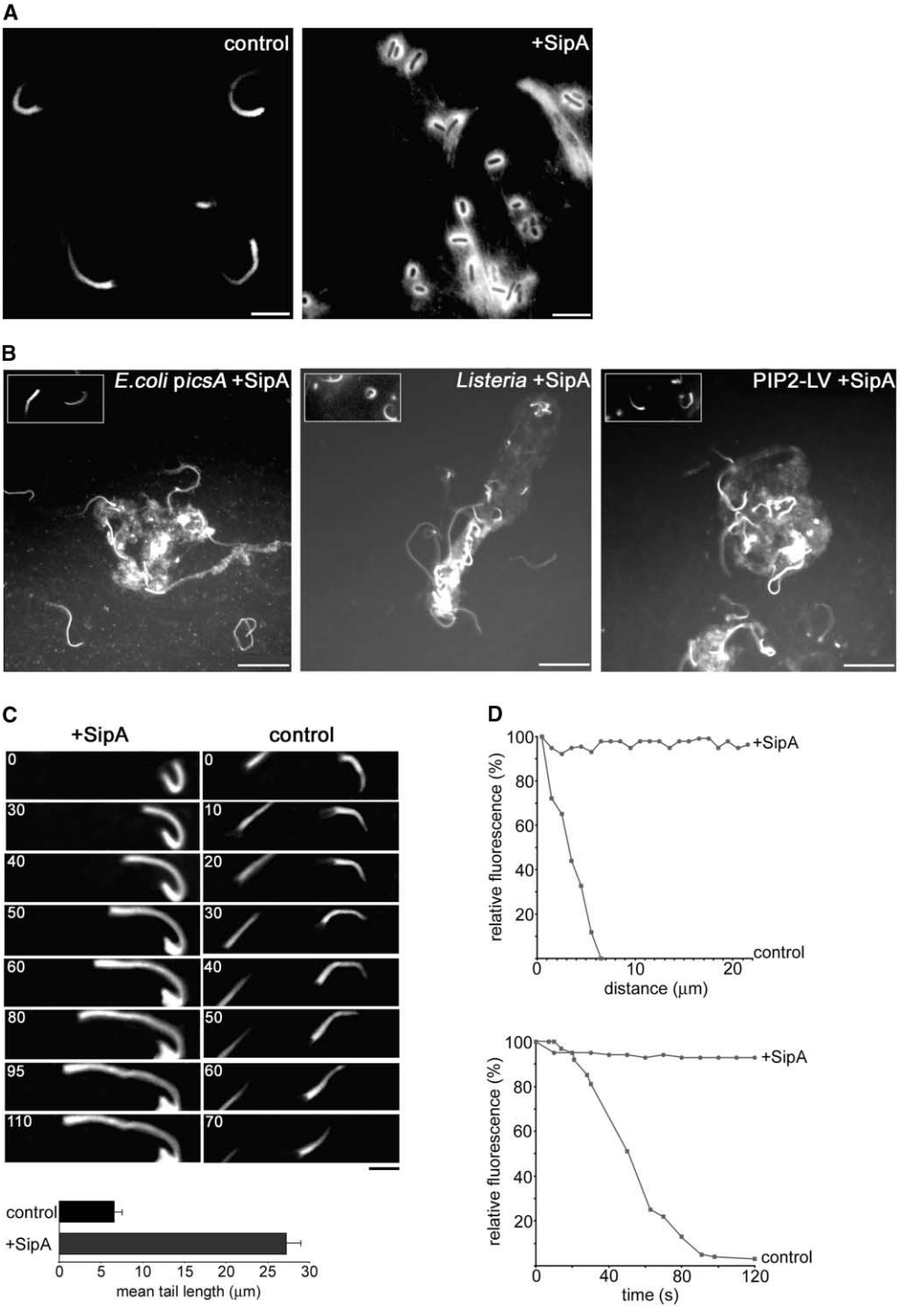

Figure 1. SipA Inhibits Actin Depolymerization in Model Comet Tails

(A) Representative fluorescence micrograph of actin comet tails (control, left) and stabilized actin "halos" (+SipA, right), formed by *E. coli* p*icsA* in *Xenopus* extract containing Rh-labeled G-actin (left), and additional SipA ([7 μM], right), visualized immediately in the Rh channel after mounting. Scale bars, 5 μm.

(B) Representative fluorescence micrographs of frozen long tails following addition of SipA (7 μM) to *Xenopus* extract containing Rh-labeled G-actin and *E. coli* p*icsA* (left, *E. coli* p*icsA* + SipA), *L. innocua* expressing *L. monocytogenes actA* (center, *Listeria* +SipA), or PIP2-enriched vesicles (right, PIP2-LV +SipA). Insets show tails formed in the absence of SipA at equivalent magnification. Images were captured in the Rh channel 5 min after mounting (~7 min after SipA addition). Scale bars, 10 μm.

(C) Sequence of fluorescence micrographs capturing tail elongation following addition of purified SipA (7 μM) (left, +SipA) to *Xenopus* extract containing Rh-labeled G-actin and *E. coli* p*icsA*. Control tails formed in the absence of SipA are shown (right, control). Panels show the same Rh channel field at the times indicated (s). t = 0 is the field immediately after mounting, ~2 min after SipA addition. Most tails formed in the

ment, actin comet tails are accepted to model the dynamic filament array within lamellipodia (Pantaloni et al., 2001) and also mimic Cdc42-dependent actin rearrangements that occur during *Salmonella* entry (Chen et al., 1996).

Recent analysis and biochemical reconstitution of such actin-based motility has revealed a central role for actin turnover in the biogenesis of lamellipodia and filopodia (Loisel et al., 1999). Polymerization is necessary but not sufficient to generate these structures, as F-actin must be actively depolymerized at sites distal from assembly zones, ensuring monomer flux to sustain continuous polymerization. Emerging evidence suggests that dynamic interplay between the major cellular depolymerization factors actin depolymerizing factor (ADF)/cofilin and gelsolin and actin-stabilizing proteins like tropomyosin is central to the control of actin turnover (Pollard and Borisy, 2003). We reasoned that actin turnover might account for the *sipA* mutant phenotype, since although the *Salmonella* effector arsenal remains adept at stimulating actin polymerization (Zhou et al., 1999a), this is apparently insufficient to generate productive membrane protrusions. This suggested that SipA might target cellular factors controlling actin depolymerization, an activity that would potentially not have been detected by the in vitro approaches used to characterize SipA-actin interaction, and additional interplay with SipC or fimbrin (Zhou et al., 1999a, 1999b; McGhie et al., 2001). To examine SipA action in a more complex environment, we initially examined the effect of purified SipA in established models of actin-based motility.

Results

SipA Inhibits Actin Depolymerization in Model Comet Tails

Actin-based motility was reconstituted in *Xenopus* extract containing rhodamine (Rh)-actin (Theriot et al., 1994). Experiments were performed in parallel with purified full-length SipA (McGhie et al., 2001), a GST-fusion to the SipA C-terminal 226 amino acids (GSTSipA-C), and this fragment cleaved from GST (SipA-C). All retain the SipA actin binding and modulating activities (Mitra et al., 2000; Zhou et al., 1999a, 1999b). Where equivalent results were obtained, these proteins are referred to generically as SipA. Purified SipA (7 μM, ~1:1 SipA:F-actin) was mixed with extract prior to the addition of *E. coli* expressing *S. flexneri icsA*. When viewed immediately by fluorescence microscopy, stabilized actin "halos" were observed tightly packed around the bacteria (Figure 1A, +SipA). Comet tails were never seen, even after prolonged incubation (>1 hr), but formed rapidly in the absence of SipA (Figure 1A, control). However, when tail formation was initiated by premixing bacteria and extract prior to the addition of SipA, many elongated tails were observed immediately after mounting (within 5 min of protein addition). These were significantly longer than those formed in control mixtures (Figures 1B and 1C; mean tail length 27.2 ± 2.1 μm [+SipA] compared to 6.6 ± 0.90 μm [control]), the most extreme examples being >50 μm. The majority of these long tails were stationary (>98%, n = 300), although elongating tails could occasionally be captured. Time-lapse microscopy of these rare events revealed that tails extended from the bacterium-proximal end at 0.1 μm/s, an average rate comparable to tails formed in control extract or those reported during bacterial infection of cultured cells (Figure 1C, +SipA; e.g., Loisel et al., 1999; Kocks et al., 1995). Image analysis revealed that Rh-actin fluorescence intensity remained constant throughout the long tails generated in the presence of SipA, whereas in control tails the signal declined rapidly with distance, consistent with efficient actin depolymerization at the bacterium-distal end (Figure 1D, upper). Similarly, when Rh-actin fluorescence intensity was quantified at a constant point within the tail over time, this also remained unchanged in the presence of SipA but declined in control tails (Figure 1D, lower). These data demonstrate that tails generated in the presence of SipA remain able to elongate but are unable to disassemble from the distal end. Once frozen, the bacteria frequently detached from the long stationary tails, which eventually clumped together (Figure 1B; *E. coli* p*icsA* + SipA). Identical results were obtained when motility was reconstituted with either *Listeria* or PIP2 lipid vesicles (Figure 1B; *Listeria* + SipA and PIP2-LV + SipA).

To establish how SipA might influence actin depolymerization in this complex system, we investigated whether SipA bound directly to the F-actin tail or acted indirectly. Actin-based motility assays are performed in small extract volumes sealed between a glass slide and coverslip, which limits protein localization by indirect immunofluorescence. Although it was possible to immunostain some tails containing cofilin and Arp2/3 as expected (not shown; David et al., 1998), the substantial loss of material and potential for artifacts was a concern. To circumvent this, purified SipA was conjugated directly to a fluorophore that couples exclusively to exposed cysteines, facilitating direct protein visualization in situ. In control in vitro assays, Oregon green-labeled SipA (OG-SipA) bound F-actin, inhibited filament depolymerization, and lowered the critical actin concentration equivalently to unmodified SipA (not shown). OG-SipA was added to extract containing *E. coli* expressing *icsA* as previously and visualized directly by time-lapse fluorescence microscopy. OG-SipA distributed uniformly throughout the elongated tails (Figure 2A, upper), and when OG-SipA fluorescence intensity was quantified at a constant point within the tail over time, this also remained constant (Figure 2A, lower), mirroring the Rh-actin signal (compare to Figure 1D, lower +SipA). Corre-

presence of SipA were already stationary at t = 0. Graph shows mean tail length scored from calibrated micrographs from three independent experiments (n > 250). Scale bar, 5 μm.

(D) Upper: Analysis of Rh-actin fluorescence intensity with respect to distance along the tail (μm) with (+SipA) and without (control) SipA. One hundred percent intensity was assigned as the signal proximal to the bacterium (d = 0) at t = 0, corrected against background. Lower: Analysis of Rh-actin fluorescence intensity with respect to time (s) at a constant point 1 μm distal from the bacterium at t = 0 with (+SipA) and without (control) SipA. One hundred percent intensity was assigned as the signal at t = 0, corrected against background.

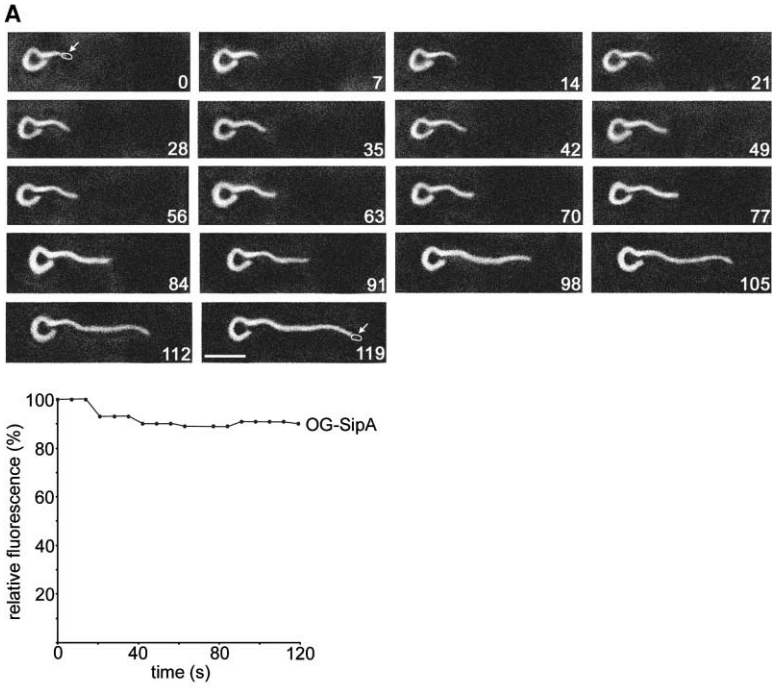

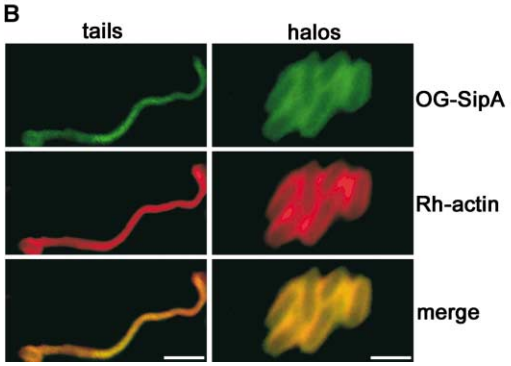

Figure 2. SipA Binds F-Actin within the Comet Tails to Inhibit Filament Depolymerization

(A) Upper: Sequence of fluorescence micrographs capturing tail elongation following addition of OG-labeled SipA (7 μM) to *Xenopus* extract containing Rh-G-actin and *E. coli* p*icsA*. Panels show the same OG channel field at the times indicated (s). t = 0 is the field immediately after mounting, ~2 min after OG-SipA addition. Most tails were stationary at t = 0. Position of the bacterium is indicated with an arrow at the beginning (t = 0) and end (t = 119) of the sequence. See Supplemental Movie at http://www.molecule.org/cgi/content/full/13/4/497/DC1. Scale bar, 5 μm. Lower: Analysis of OG fluorescence intensity in the series (upper) with respect to time (s) at a constant point 1 μm distal from the bacterium at t = 0. One hundred percent intensity was assigned as the fluorescence intensity at t = 0, corrected against background.

(B) Localization of OG-SipA (green) and Rh actin (red) within long tails formed following addition of OG-SipA (7 μM) to *Xenopus* extract containing Rh G-actin and *E. coli* p*icsA* (left, tails), and actin "halos" formed after addition of *E. coli* p*icsA* to *Xenopus* extract containing OG-SipA (right, halos). Coincident Rh-actin and OG-SipA appears yellow in merge. Scale bars, 5 μm (left) and 2 μm (right).

spondingly, when both OG-SipA and Rh-actin fluorescence were simultaneously visualized in long tails and halos, OG-SipA and Rh-actin fluorescence were coincident (Figure 2B), showing that OG-SipA bound uniformly throughout the tail, where it remained stably associated with F-actin. These findings suggested that by binding to F-actin, SipA inhibits actin depolymerization in a complex system. Remarkably similar "frozen" tails were observed when ADF/cofilin was depleted from *Xenopus* extract (Rosenblatt et al., 1997), a factor subsequently shown to be essential for bacterial motility and actin turnover (Loisel et al., 1999).

SipA Prevents ADF/Cofilin-Directed Actin Depolymerization

In vitro assays of actin dynamics were next used to investigate the possibility of interplay between SipA and ADF/cofilin as suggested by the elongated tail phenotype. ADF/cofilin binds both monomeric (G-) and F-actin (Renoult et al., 1999). Upon F-actin binding, ADF/cofilin triggers a change in helical filament twist (Bamburg et al., 1999; McGough et al., 1997), inducing depolymerization by increasing the pointed end monomer dissociation rate (Carlier et al., 1997) and by severing F-actin (Moriyama and Yahara, 1999). A sedimentation assay was initially used to assess whether purified SipA could protect F-actin from ADF/cofilin-directed depolymerization. When ADF was mixed with F-actin at pH 8, significant filament disassembly occurred, i.e., less F-actin pelleted (Figure 3A, compare tracks 1 and 2), whereas the less potent cofilin induced only limited filament depolymerization under identical conditions (Yeoh et al., 2002) (Figure 3A, compare tracks 1 and 10). DNase I sequesters G-actin, artificially biasing the G-F actin equilibrium in favor of monomers (Hitchcock et al., 1976) (Figure 3A, compare tracks 1 and 3). When incubated with DNase I, ADF/cofilin-directed F-actin depolymerization was further enhanced, as released G-actin is sequestered limiting filament repolymerization in vitro (Figure 3A, compare tracks 2 and 4, and tracks 10 and 11). When ADF/cofilin was added to an equimolar SipA-F-actin complex, F-actin depolymerization was strongly inhibited, even in the presence of DNase I (Figure 3A, compare tracks 3 and 7, tracks 4 and 9, tracks 10 and

12, and tracks 11 and 13). These data suggest that SipA protects F-actin from ADF/cofilin-directed depolymerization in vitro.

The effect of SipA on ADF/cofilin-directed F-actin depolymerization kinetics was investigated using pyrene-actin, a fluorescent derivative that has higher fluorescence intensity as filaments than as monomers. Following the addition of excess ADF/cofilin, F-actin rapidly depolymerized (Figure 3B, control), whereas F-actin prebound to SipA was highly stable (Figure 3B, +SipA, 10 min). Even when SipA-F-actin complexes were incubated for prolonged periods, they remained resistant to subsequent ADF/cofilin-directed depolymerization (Figure 3B, +SipA, 1 day and 1 week). These findings supported the cosedimentation data, showing that SipA confers immediate protection from ADF/cofilin activity, and additionally demonstrate the remarkable stability of SipA-F-actin complexes.

To further confirm these data, Rh-labeled F-actin was visualized directly by fluorescence microscopy (Xu et al., 1999) (Figure 3C, control −ADF). While Rh-F-actin was completely depolymerized by ADF/cofilin (Figure 3C, control +ADF), Rh-F-actin preincubated with an equimolar concentration of SipA remained intact upon addition of ADF/cofilin, even upon sustained incubation (Figure 3C, +SipA [1:1]). When substoichiometric concentrations of SipA were added, only short resistant filaments were observed, consistent with limited SipA availability (Figure 3C, + SipA [1:5]). In agreement with the phenotype of SipA-bound actin comet tails (Figures 1 and 2), the combined data from three independent in vitro assays demonstrate that SipA renders F-actin resistant to ADF/cofilin-directed depolymerization.

SipA Displaces ADF/Cofilin from F-Actin

To further investigate the basis for SipA-directed inhibition of ADF/cofilin-directed actin depolymerization, we used cosedimentation to determine whether SipA inhibited ADF/cofilin F-actin binding. At pH6, ADF/cofilin binds to F-actin without inducing filament depolymerization, i.e., binding and depolymerization are artificially uncoupled. F-actin remained intact at pH 6, and purified SipA and ADF were both soluble (Figure 4A, tracks 4–6), retaining their actin binding activity (Figure 4A, tracks 1 and 2). In contrast to its activity at pH 8, ADF induced no significant filament depolymerization (compare Figure 4A, track 1 [pH 6] to Figure 3A, track 2 [pH 8]). However, when SipA was preincubated with F-actin at saturating concentrations (1:1), subsequent binding of ADF/cofilin to F-actin was prevented [Figure 4A, track 3 (SipA + F-actin, then ADF/cofilin)]. Even when the amount of ADF/cofilin was increased, no SipA was displaced from F-actin (not shown). These findings suggested that SipA blocks F-actin depolymerization by preventing ADF/cofilin from binding to the filament.

To examine whether F-actin binding by ADF/cofilin and SipA is mutually exclusive, SipA was mixed with F-actin prebound to a saturating concentration of ADF/cofilin at pH 6. Unexpectedly, SipA displaced ADF/cofilin at stoichiometric concentrations. A SipA-F-actin complex partitioned away from ADF/cofilin (Figure 4B, left, track 8), as ADF/cofilin was displaced from the filament (Figure 4B, left, compare ADF distribution in tracks 7 and 8). Isothermal titration calorimetry (ITC) was applied to investigate whether a difference in relative affinity might account for this ability of SipA to displace ADF/cofilin from F-actin. ITC experiments were performed by titrating purified SipA into a reservoir containing F-actin. SipA interacted strongly with F-actin in the presence of excess ATP (Figure 4B, right). From the derived affinity constant ($0.38 \pm 0.24 \times 10^6\ M^{-1}$), SipA apparently has significantly higher affinity than ADF for ATP•F-actin (ADF $K_d = 10 \times 10^6\ M^{-1}$; Carlier et al., 1997), indicating that relative affinity might contribute to the mechanism. These combined data show that SipA can prevent depolymerization not only by excluding ADF/cofilin from F-actin but also by displacing ADF/cofilin pre-bound to F-actin in vitro.

To further these in vitro observations (Figures 4A and 4B), we investigated whether SipA could displace ADF from actin comet tails induced by *E.coli* expressing *icsA*. To facilitate simultaneous real-time visualization of OG-SipA and ADF, purified ADF was labeled with rhodamine (Rh) on its surface-exposed cysteine residue. This Rh-ADF derivative bound and depolymerized F-actin with equivalent activity to unmodified ADF (not shown). The Rh-ADF concentration was titrated such that tail length was equivalent to that observed in unsupplemented extract, as excess Rh-ADF decreases tail length due to increased actin depolymerization (Rosenblatt et al., 1997). In the absence of SipA, Rh-ADF localized throughout the tails (Figure 4C, −SipA), in agreement with cofilin immunolocalization in cells after *Listeria* infection (David et al., 1998). When OG-SipA was added following initiation of tail formation in the presence of Rh-ADF, extended tails were again observed. These tails labeled strongly with OG-SipA, but no longer contained Rh-ADF (Figure 4C, +SipA). These data demonstrate that SipA inhibits actin depolymerization both by excluding and displacing ADF/cofilin from F-actin.

SipA Protects F-Actin from Gelsolin-Directed Severing and Reanneals Capped Filaments

In addition to ADF/cofilin, another cellular ABP gelsolin also influences actin turnover in vivo by severing F-actin and capping the barbed ends (McLaughlin et al., 1993). Although gelsolin is apparently not essential for *Listeria* motility in extracts (Loisel et al., 1999), gelsolin-transfected cell lines display an increase in bacterial motility (Laine et al., 1998). Gelsolin null cells also exhibit delayed filopodial retraction, suggesting crosstalk with Rac GTPase signaling (Lu et al., 1997).

To investigate potential interplay between SipA and gelsolin, we utilized a sedimentation assay to monitor gelsolin-directed F-actin severing. Intact F-actin and short severed filament fragments differentially segregate into the pellet and supernatant, respectively. While gelsolin alone induced efficient F-actin severing in vitro (1:2 gelsolin:actin induced 60% severing; Figure 5A, upper, control), SipA-F-actin (1:1) was protected from severing, even after extended incubation (Figure 5A, upper, +SipA). This was independent of gelsolin concentration, as SipA still shielded F-actin when gelsolin was present at nonphysiological stoichiometric (1:1:1) ratios (Figure 5A, lower). However, in contrast to ADF/cofilin (Figure 4B, left), SipA and gelsolin binding to F-actin was not

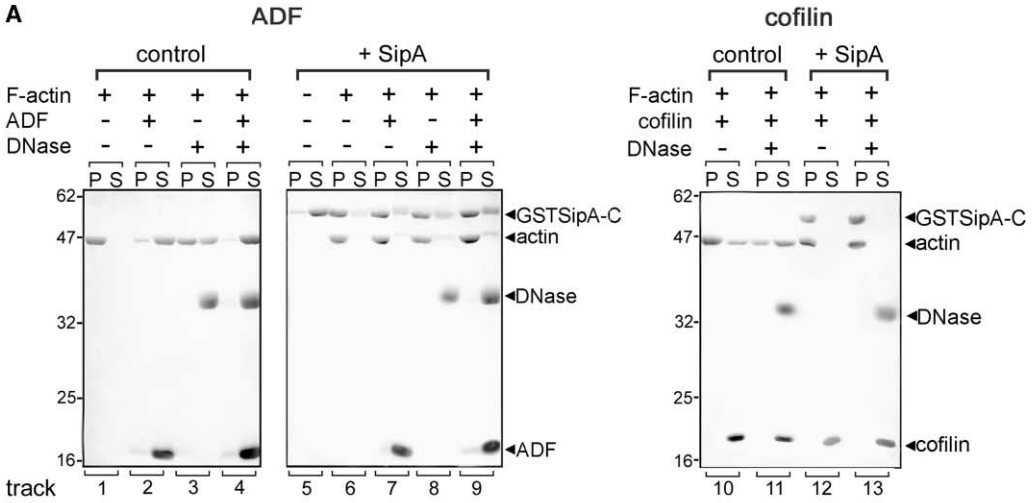
A
ADF
cofilin
control
+ SipA
F-actin
ADF
cofilin
DNase
P S
62
47
32
25
16
GSTSipA-C
actin
DNase
ADF
cofilin
track
1 2 3 4 5 6 7 8 9 10 11 12 13

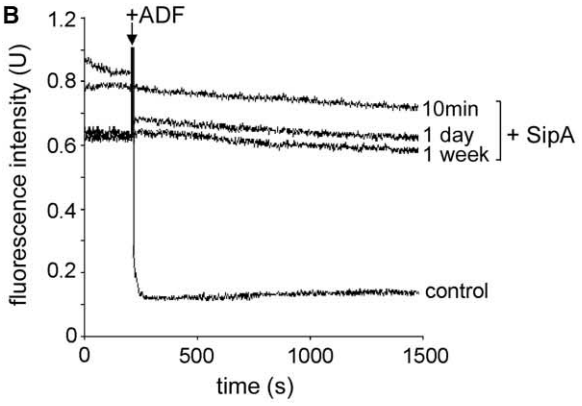
B
+ADF
fluorescence intensity (U)
1.2
0.8
0.6
0.4
0.2
0
10min
1 day
1 week
+ SipA
control
0
500
1000
1500
time (s)

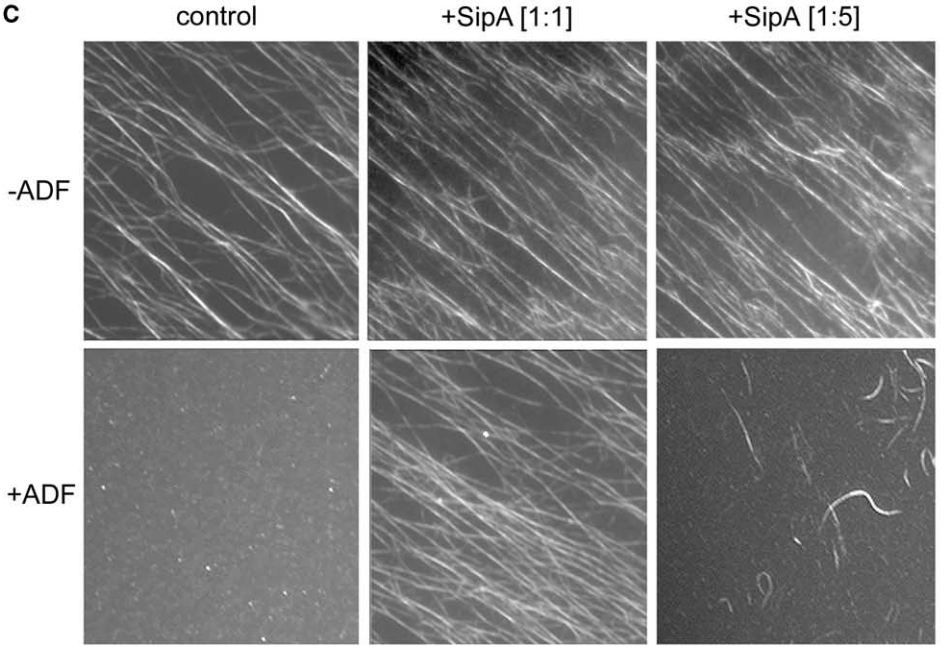
C
control
+SipA [1:1]
+SipA [1:5]
-ADF
+ADF

mutually exclusive, as even though severing was prevented, gelsolin bound SipA-F-actin (Figure 5A, upper, +SipA). As previously (Figure 3B), pyrene-labeled F-actin was employed to investigate the effect of SipA on the kinetics of gelsolin-directed severing. Addition of gelsolin to preassembled pyrene F-actin induced a fluorescence intensity decrease, which results both from initial binding of gelsolin and subsequent rapid pointed-end depolymerization, as described previously (Figure 5B, control; Kinosian et al., 1996). SipA inhibited gelsolin-directed severing, as the percentage of pyrene-labeled F-actin remained constant (Figure 5B, +SipA). These data show that although SipA and gelsolin binding is not mutually exclusive, SipA protects F-actin from gelsolin-directed severing.

Substoichiometric gelsolin concentrations nucleate actin polymerization in vitro by binding G-actin (Kwiatkowski, 1999). SipA also bound to gelsolin-nucleated F-actin (Figure 6A [i], tracks 1 and 2), and blocked ADF/cofilin-directed depolymerization of gelsolin-nucleated and capped F-actin (Figure 6A [ii], compare tracks 3 and 5, and tracks 4 and 6]. However, the proportion of sedimented actin apparently increased after SipA addition to F-actin fragments capped with gelsolin (Figure 6A [i], compare partitioning in tracks 1 and 2). This suggested that either SipA binding significantly increased gelsolin-capped filament density or SipA reannealed short gelsolin-capped F-actin fragments. To distinguish these possibilities, SipA or control buffer was incubated with F-actin fragments (2 μM), which had been severed and capped with gelsolin. Solution viscosity significantly increased following SipA addition (2 μM), and sedimentation and densitometry revealed that 95% of the actin pelleted in the presence of SipA, whereas only 45% sedimented with control buffer (Figure 6B, left). Consistent with the findings that gelsolin and SipA simultaneously bind F-actin (Figure 5A, +SipA), gelsolin also cosedimented with actin and SipA in this assay. Indeed, densitometric analysis revealed that cosedimented gelsolin increased as a function of gelsolin concentration until saturation (Figure 6B, right). This indicates that SipA interacts with gelsolin-capped F-actin fragments without displacing gelsolin. Transmission electron microscopy was used to visualize these mixtures prior to sedimentation. Control samples exclusively contained uniform short severed F-actin fragments, which averaged 40 ± 2 nm (n = 200) in length (Figure 6C, control). In contrast, only much longer filaments (averaging 550 ± 27 nm [n = 148]) were observed in the viscous solutions containing SipA (Figure 6C, +SipA), which were thickened and straightened consistent with SipA binding (McGhie et al., 2001; Zhou et al., 1999a). These data suggest that SipA is additionally able to reanneal F-actin fragments severed and capped by the cellular ABP gelsolin.

Discussion

Invasive *Salmonella* delivers two ABPs, SipA and SipC (Zhou et al., 1999a; Hayward and Koronakis, 1999), into target mammalian cells to promote bacterial internalization. The actin binding and modulating activities of SipA have been extensively characterized in isolation (Zhou et al., 1999a, 1999b; Mitra et al., 2000; McGhie et al., 2001; Galkin et al., 2002), whereas this study describes SipA function in a complex system, akin to the eukaryotic target cell environment. We show that SipA short-circuits actin turnover by blocking host actin depolymerization and severing directed by ADF/cofilin and gelsolin, respectively, although SipA binding excludes ADF/cofilin but not gelsolin from F-actin. Perhaps most remarkably, SipA also displaces ADF/cofilin prebound to F-actin, to our knowledge the first example of a known ABP with such activity. The study of novel bacterial activities has promoted fundamental advances in cell biology; for example, the characterization of *Listeria* ActA allowed the identification of the homologous WASP/WAVE Arp2/3 activators (Welch et al., 1998; Machesky and Insall, 1998). By analogy, these SipA activities might also provide new insights into host cell biology.

How might these SipA activities contribute to bacterial entry? *Salmonella* mutants lacking *sipA* enter cells less efficiently (Zhou et al., 1999a). Only diffuse actin rearrangements occur, and the cellular F-actin content decreases 80% compared to controls (Higashide et al., 2002). These phenotypes indicate that even though multiple *Salmonella* effectors induce actin polymerization, the resultant structures remain susceptible to disassembly by cellular factors (Figure 7A, left). Our data show that SipA inhibits the pivotal host proteins that control actin depolymerization. Such activity would concentrate polymerization at free barbed filament ends nucleated beneath the plasma membrane by SipC (Hayward and Koronakis, 1999) or perhaps cellular Arp2/3. This effect would be further accentuated by SipA-directed reannealing of gelsolin-capped F-actin fragments, which decreases the total number of free filament ends (Figure 7A, right). Although SipA completely arrests actin turnover in *Xenopus* extract, where the cellular factors are rapidly out-titrated, it is likely that a more localized effect occurs upon SipA delivery in vivo. This would ensure that sufficient G-actin remains available at more distal sites to maintain polymerization, although as SipA induces polymerization at G-actin levels below the critical concentration (Galkin et al., 2002), assembly might even

Figure 3. SipA-Bound F-Actin Is Resistant to ADF/Cofilin-Directed Depolymerization

(A) Left: Cosedimentation of F-actin (1 μM) incubated with purified ADF (4 μM), DNase (2 μM), or both (pH 8, 90 min), with additional GSTSipA-C (1 μM, 10 min preincubation, RT) where indicated (+SipA). Pellets (P) and supernatants (S) were analyzed by Coomassie blue-stained SDS-PAGE. Right: Cosedimentation (as left) substituting purified cofilin (4 μM) for ADF. Track numbers are provided for reference.

(B) Effect of ADF (4 μM) on pyrene-F-actin alone (1 μM, control) or preincubated with SipA (1 μM; 10 min, 1 day, 1 week; RT) prior to the assay. Pyrene fluorescence intensity is plotted against incubation time, with arrow indicating ADF addition.

(C) Fluorescence micrographs of Rh-labeled F-actin (5 μM) fixed after incubation (2 min, RT) with (+ADF) or without (−ADF) ADF (8 μM), alone (control), or after preincubation (2 min, RT) with SipA (5 μM, +SipA [1:1]; 1 μM, +SipA [1:5]).

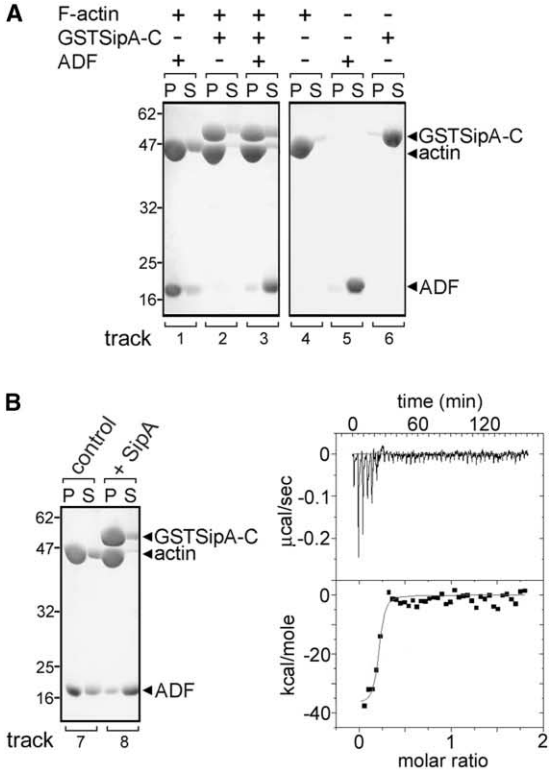

Figure 4. SipA Displaces ADF/Cofilin from F-Actin

(A) Cosedimentation of F-actin (2 μM), incubated (pH 6, 20 min, RT) with GSTSipA-C (2 μM) and ADF (2 μM) as indicated. Pellets (P) and supernatants (S) were analyzed by Coomassie blue-stained SDS-PAGE. Equivalent results were obtained when cofilin was substituted for ADF.

(B) Left: Cosedimentation of F-actin (2 μM) prebound to ADF (2 μM [pH 6], 20 min, RT; control), and after incubation with GSTSipA-C (2 μM). Right: SipA-F-actin affinity measured by ITC. SipA was titrated into F-actin in F buffer. Upper panel shows raw data for sequential injection of 5 μl vol SipA (45 μM) into 2 ml F-actin (5 μM). Lower panel shows dilution-corrected integrated heat data with a fit according to a single binding site model.

(C) Dual channel fluorescence micrographs of tails generated by *E. coli picsA* in *Xenopus* extract containing Rh-ADF (−SipA) and with OG-SipA (+SipA). Bacteria were visualized by phase contrast microscopy and are shown merged with the Rh-actin channel.

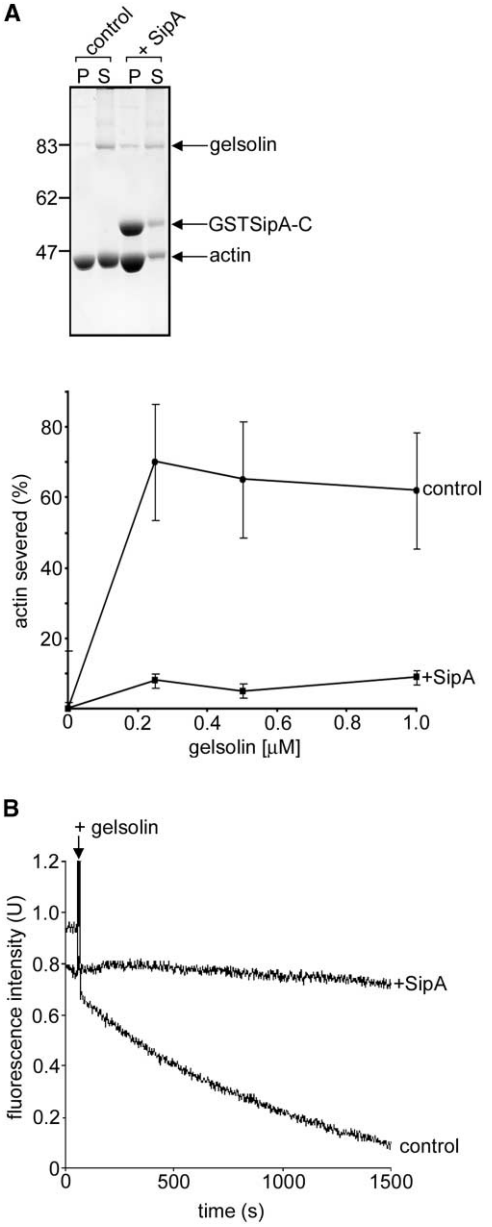

Figure 5. SipA Prevents Gelsolin-Directed F-Actin Severing

(A) Upper: Cosedimentation of F-actin alone (2 μM, control) or premixed (10 min, RT) with GSTSipA-C (both 2μM, +SipA), then incubated with gelsolin (1 μM, 30 min, RT). Pellets (P) and supernatants (S) were analyzed by Coomassie blue-stained SDS-PAGE. Lower: Effect of SipA on gelsolin-directed actin severing. F-actin alone (1 μM) or premixed (10 min, RT) with GSTSipA-C (both 1 μM, +SipA) was incubated with varied concentrations of gelsolin (0–1 μM, 30 min, RT). Pellets and supernatants from cosedimentation were analyzed by Coomassie blue-stained SDS-PAGE and densitometry. Graph shows the percentage actin severed as a function of gelsolin concentration in the presence (+SipA) and absence (control) of SipA. The minor contribution of longer severed filaments which sediment with intact F-actin was discounted.

(B) Effect of gelsolin on pyrene-F-actin alone (2 μM, control) or premixed with SipA (2 μM, 10 min, RT; SipA). Fluorescence intensity is plotted against incubation time, with arrow indicating addition of gelsolin (0.5 μM).

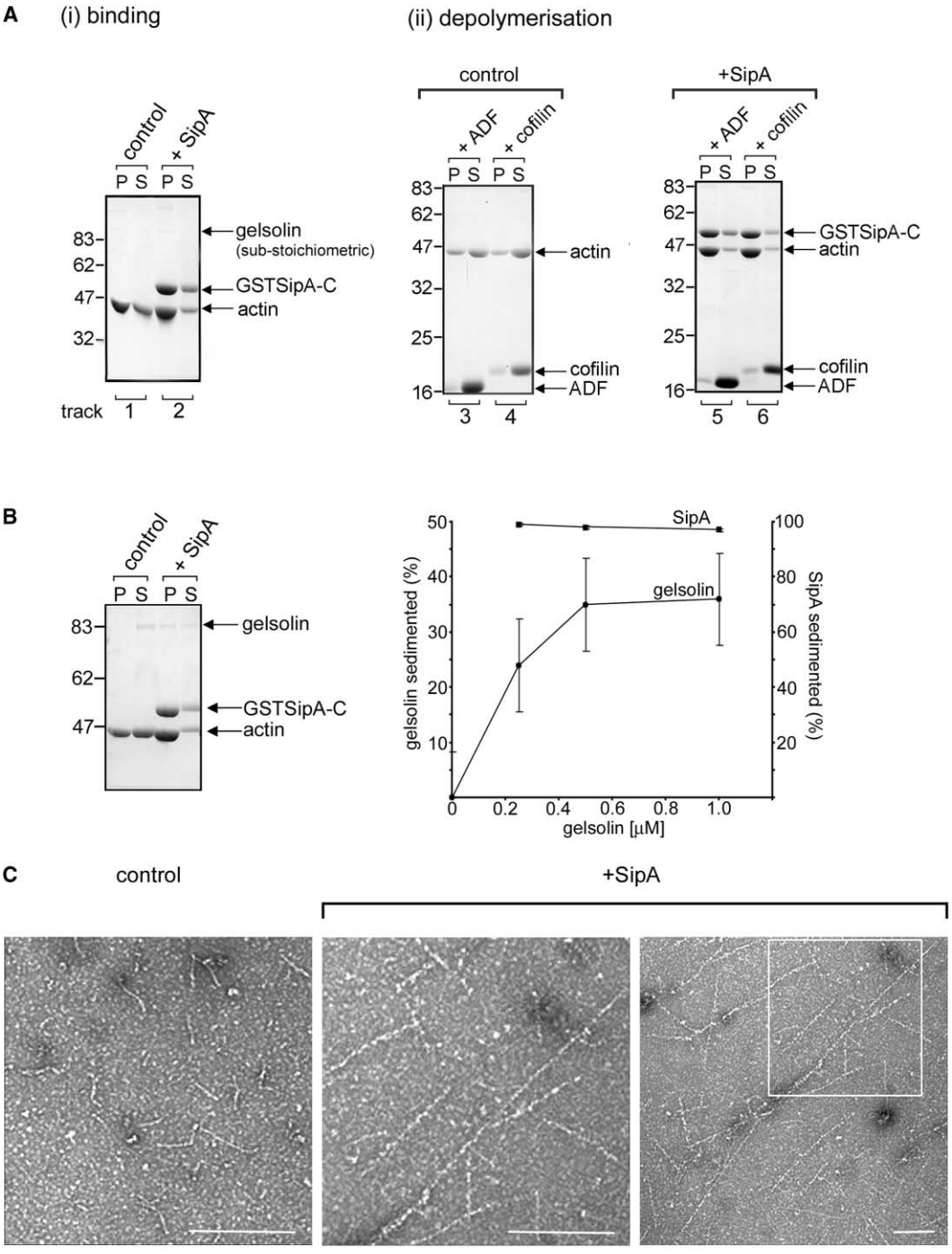

Figure 6. SipA Binds Gelsolin-Nucleated F-Actin, Protects It from ADF/Cofilin Depolymerization, and Reanneals Gelsolin-Severed Filament Fragments

(A) Left: Cosedimentation of gelsolin-nucleated F-actin (2 μM F-actin, 0.01 μM gelsolin) alone (control), or mixed with GSTSipA-C (2 μM). Pellets (P) and supernatants (S) were analyzed by Coomassie blue-stained SDS-PAGE. Substoichiometric concentrations of gelsolin are below the detection threshold for Coomassie blue staining. Right: Cosedimentation of a gelsolin-nucleated F-actin-GSTSipA-C complex (2 μM F-actin, 2 μM GSTSipA-C, 0.01 μM gelsolin), after incubation with ADF or cofilin (8 μM, 90 min, RT; as indicated). Pellets and supernatants were analyzed by Coomassie blue-stained SDS-PAGE.

(B) Left: Cosedimentation of F-actin (2 μM) mixed with gelsolin (0.5 μM, 30 min, RT) alone (control) or after addition of GSTSipA-C (2 μM, 5 min, RT, +SipA). Pellets and supernatants were analyzed by Coomasie blue-stained SDS-PAGE. Right: Cosedimentation of SipA-gelsolin-F-actin complexes. F-actin was mixed with varied concentrations of gelsolin (1 μM F-actin, 0.1–1 μM gelsolin, 1 hr, RT), and GSTSipA-C was added (1 μM, 10 min, RT). After centrifugation, pellets were analyzed by Coomassie blue-stained SDS-PAGE and densitometry, and the percentage gelsolin and SipA sedimented was determined. Values were corrected for gelsolin pelleted in the absence of SipA at each concentration (<5% input) or for SipA sedimented in the absence of gelsolin and actin (<3%), as appropriate. Graph shows percentage of gelsolin (left axis) and SipA (right) sedimented as a function of gelsolin concentration.

(C) Transmission electron micrographs of F-actin mixed with gelsolin (2 μM F-actin, 0.5 μM gelsolin) following incubation (1 hr, RT) and clarification (100,000 g, 15 min, control), and after GSTSipA-C addition (2 μM, further 1 hr, RT, +SipA). Scale bars, 200 nm.

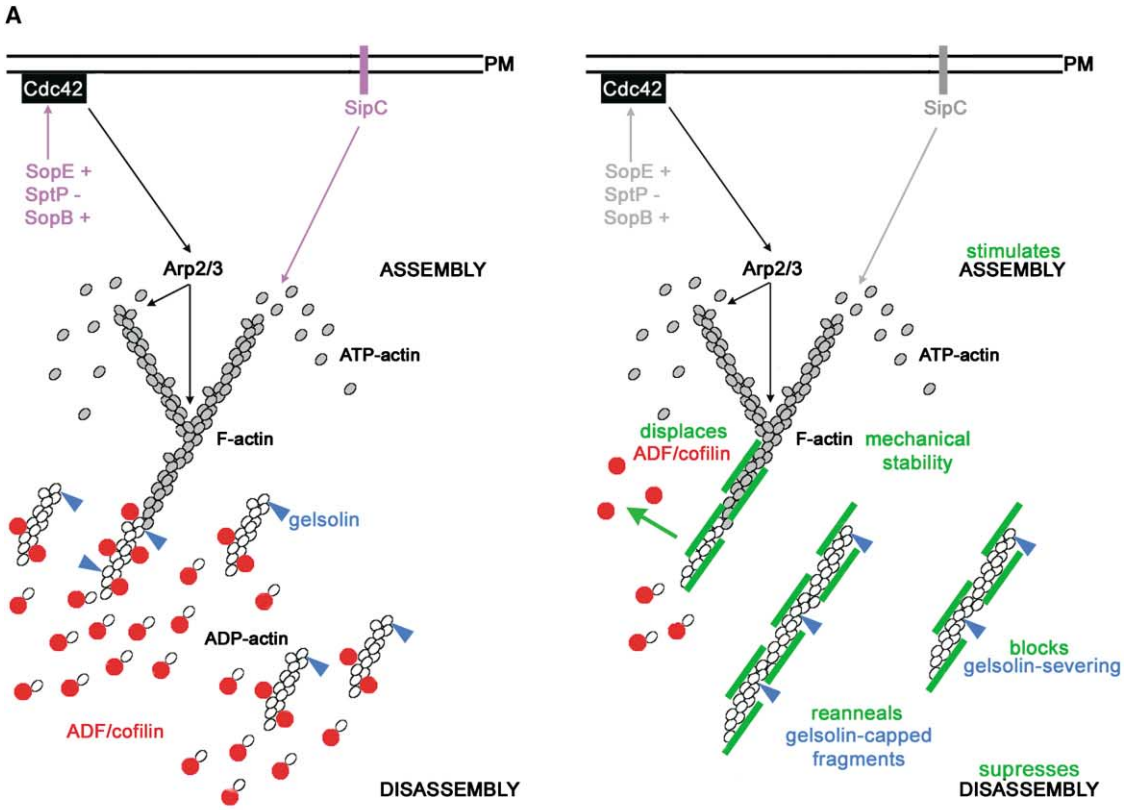

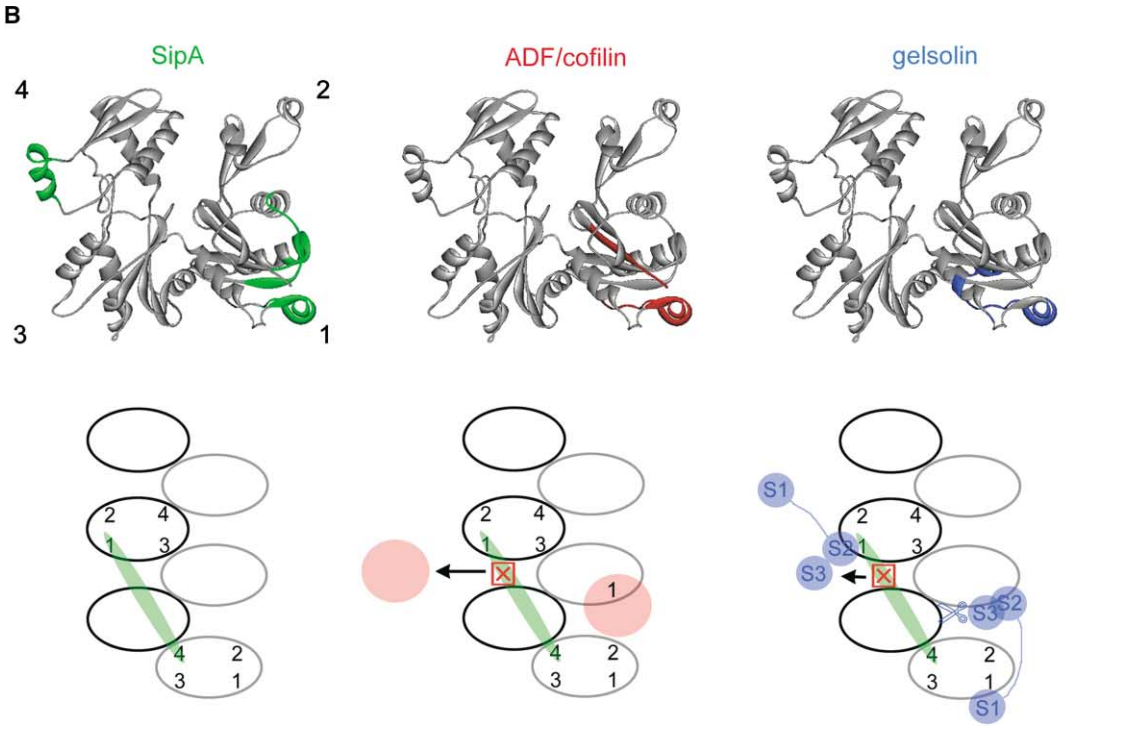

Figure 7. Consequences of SipA-Directed Inhibition of ADF/Cofilin and Gelsolin

(A) Left: Schematic of actin turnover during cell entry by a *Salmonella sipA* mutant. Actin polymerization is nucleated beneath the host cell plasma membrane (PM) by delivered effectors (magenta), both directly by SipC and by SopE(2)/SopB stimulation of Arp2/3, signaling subse-

occur if free monomer flux from pointed-end disassembly was completely eliminated. This model would account for the observed rapid burst of localized submembranous actin polymerization (Finlay et al., 1991), fueling efficient formation of lamellipodia and filopodia proximal to the adherent bacterium.

Electron microscopy and helical image analysis provided first insights into the structure of the SipA-C-F-actin complex (Galkin et al., 2002). SipA-C binds to F-actin as a tubular molecule (Mitra et al., 2000) and contacts actin in two distinct regions, the helix of subdomain 4 and an undefined region of the C terminus located within subdomain 1 (Figure 7B, upper, SipA; Galkin et al., 2002). In assembled filaments, SipA is proposed to connect subdomain 4 of one actin monomer to subdomain 1 of another monomer on the opposite long-pitch helical strand (Figure 7B, lower, SipA). The structure of both cofilin- and gelsolin-F-actin complexes have been analyzed (McGough et al., 1997; Burtnick et al., 1997), and the ABP binding sites on actin delineated by exhaustive mutagenesis and crosslinking (Sheterline et al., 1998). In common with SipA, both ADF/cofilin and gelsolin contact actin subdomain 1 (Figure 7B, upper; ADF/cofilin and gelsolin). When SipA and cofilin are modeled bound to F-actin simultaneously, SipA-C obstructs the cleft that accommodates cofilin (Figure 7B, lower, ADF/cofilin). This is consistent with our findings demonstrating that SipA excludes ADF/cofilin from F-actin. Whether SipA can additionally counteract the helical twist induced by cofilin requires further investigation, although as SipA binding does not detectably alter filament architecture (Galkin et al., 2002), this perhaps favors simple steric hindrance. Similarly, whether SipA-directed ADF/cofilin displacement is exclusively a consequence of differential affinity requires further investigation. Our data also show that while SipA counteracts gelsolin-directed F-actin severing, F-actin binding is not mutually exclusive. This implies that, in the presence of SipA, gelsolin subfragment 2 (S2) can still contact actin subdomain 1. However, when SipA and gelsolin are both bound to F-actin, the cleft into which S3 inserts to initiate conformational changes in gelsolin required for severing is nevertheless occupied by SipA (Figure 7B, lower, gelsolin). Unlike SipA, ADF/cofilin competes with gelsolin S2 and S3 for binding to F-actin, suggesting that their respective subdomain 1 contacts must subtly differ.

Our modeling (Figure 7) combining the available data from electron microscopy, mutagenesis, and crosslinking of ABP-actin complexes is strongly supported by the recent data of Lilic and coworkers (2003) describing the high resolution structure of a SipA C-terminal fragment (residues 497–669). Unlike other bacterial effectors that are convergent mimics of their eukaryotic counterparts (Stebbins and Galán, 2001), this highly helical SipA F-actin binding fragment does not resemble any known actin binding fold. The polarized molecular surface is proposed to mediate actin binding via electrostatic interactions, while flexible nonglobular arms extend to contact subdomains 1 and 4 of opposing actin monomers (Lilic et al., 2003), and perhaps act as a "molecular staple" to stabilize the filament. These findings are consistent with and complement our model for how ADF/cofilin might be excluded while gelsolin is accommodated in a SipA-F-actin complex. The insights provided by this crystal structure, in combination with those of ADF/cofilin and gelsolin (Burtnick et al., 1997; Leonard et al., 1997), will provide new opportunities to define the underlying molecular mechanisms.

In addition to inhibiting actin depolymerization, SipA reanneals gelsolin-capped actin filament fragments. Our findings establish that the annealed complex contains both SipA and gelsolin but do not yet reveal the molecular mechanism of annealing. It seems likely from our electron microscopy and biochemical analysis and the recent structural data (Lilic et al., 2003) that SipA laterally staples or splices filament junctions, but whether gelsolin is retained only at filament termini or at every junction remains to be determined. Provocatively, the cellular ABP tropomyosin also reanneals gelsolin-capped F-actin fragments (Nyåkern-Meazza et al., 2002), and is similarly proposed to antagonize the activity of ADF/cofilin (Cooper, 2002). Indeed, like SipA, tropomyosin also stabilizes F-actin (Wegner, 1982), and protects filaments from gelsolin- and ADF/cofilin-directed depolymerization (Ono and Ono, 2002; Bernstein and Bamburg, 1982). However, there are also significant differences in that homodimeric tropomyosin cooperatively binds to the side of F-actin, spanning six to seven actin mono-

quently reversed by SptP. This leads to rapid addition of ATP-G-actin (gray) at membrane-proximal and more distal barbed ends. Filaments age by ATP hydrolysis and phosphate dissociation (gray subunits turn white). ADF/cofilin (red) promotes phosphate dissociation, severs ADP-F-actin, and promotes ADP-G-actin dissociation (white) from pointed ends. Gelsolin (blue) binds F-actin, directs filament severing, and caps their barbed ends. In *sipA* mutants, newly polymerized filaments are thus rapidly disassembled. Right: Schematic of actin turnover blocked by wild-type *Salmonella*. Delivered SipA (green) stimulates actin assembly by lowering the critical monomer concentration and mechanically stabilizes F-actin. SipA-bound F-actin is protected from ADF/cofilin-depolymerization and gelsolin-directed severing. SipA displaces ADF/cofilin from F-actin to prevent disassembly. Preexisting gelsolin-capped F-actin fragments are reannealed, decreasing the number of free ends. This local inhibition of actin depolymerization ensures focused submembranous barbed-end assembly occurs and promotes persistence of pathogen-induced actin rearrangements.

(B) Comparison of SipA, cofilin, and gelsolin actin binding sites. Upper: SipA (green, left), ADF/cofilin (red, center), and gelsolin (blue, right) contact sites mapped onto G-actin (subdomains [SD] indicated 1–4). Lower: Models of ABPs bound to F-actin. Individual actin monomers are depicted as ovals, with the two-pitch helical strand indicated in gray and black. Left: SipA-C (green) connects SD4 of one actin monomer with SD1 of another monomer on the opposite strand. Center: ADF/cofilin (red) bound to F-actin alone (right strand) and in the presence of SipA (green) left strand. Bound SipA excludes ADF/cofilin from the SD1 binding site (red cross). Right: Gelsolin (blue) bound to F-actin alone (right strand) and in the presence of SipA (green) left strand. Gelsolin consists of two tandem-homologous halves (segments [S] 1–3 and 4–6). For clarity S4–6 have been omitted from the opposing filament strand. S2 binds SD1, triggering S3 to enter the cleft. This initiates a conformational change allowing S1 to lodge between two monomers along the longitudinal axis and S4–6 to reach across the filament to engage a monomer on the other strand (not shown), facilitating filament severing. Bound SipA (green) allows S2 binding but excludes S3 (red cross), allowing gelsolin to bind but not sever filaments.

mers (Araya et al., 2002), and localizes preferentially to the base of lamellipodia rather than at assembly zones (DesMarais et al., 2002). Furthermore, although tropomyosin antagonizes ADF/cofilin, unlike SipA tropomyosin cannot displace ADF/cofilin from actin (Ono and Ono, 2002). Thus, although there appear to be some similarities between the only known cellular ABP that counteracts ADF/cofilin and gelsolin activity and SipA, further comparative analysis is now required.

Despite these insights into SipA function, how SipA-F-actin complexes depolymerize in vivo remains unresolved. Disassembly is not directed by ADF/cofilin, gelsolin, or apparently by any other eukaryotic protein at high efficiency, as the complex remains intact in *Xenopus* extract. It is possible that the action of a further bacterial effector/s is required, either to depolymerize these structures directly or to activate a cellular activity dormant in extract. Another possibility is that SipA is targeted for degradation by cellular machinery, as has recently been suggested for *Salmonella* SopE and SptP (Kubori and Galán, 2003). Alternatively, these stabilized filaments might remain in contact with *Salmonella*-containing vacuoles, acting as physical supports or interactive scaffolds for further effectors that promote intracellular survival (Waterman and Holden, 2003). It is nevertheless clear that SipA is a remarkable example of a multifunctional bacterial ABP mimic that not only promotes actin polymerization in host cells but also counteracts cellular disassembly mechanisms to induce the rapid formation of membrane ruffles, an activity central to the virulence of this bacterial pathogen.

Experimental Procedures

More detailed experimental procedures are provided in the Supplemental Data at http://www.molecule.org/cgi/content/full/13/4/497/DC1.

Cloning, Expression, and Purification of Recombinant Proteins

pGSTAC encoding SipA residues 459–685 was generated by PCR from the *S. typhimurium* SJW1103 chromosome (Yamaguchi et al., 1984) and cloning into pGEX-2T (Amersham). Transformed *E. coli* BL21(DE3) cells (Studier and Moffat, 1986) were grown to OD_{600} = 1 and induced (IPTG, 2 hr). Cells were pelleted, resuspended (10 mM Tris-Cl [pH 7.4], 150 mM NaCl) and lysed in a French Press (82,800 kPa, Aminco). Lysates were clarified (100,000 g, 2 hr), and GSTSipA-C purified from the soluble fraction using Glutathione Sepharose 4B (Amersham). Eluted GSTSipA-C was dialyzed (20 mM Tris-HCl [pH 7.4]) and further purified by anion exchange chromatography (Q-Sepharose, Amersham). SipA-C was cleaved from GST with thrombin (Zhou et al. 1999a, 1999b). SipA was purified as described by McGhie et al. (2001).

pT7ADF and pT7COF encoding ADF and cofilin, respectively, were generated by PCR from appropriate human cDNA plasmids (I.M.A.G.E. Consortium) and cloning into pET3a (Novagen). ADF/cofilin was purified as described by Pope et al. (2000).

Fluorescence Labeling

SipA/GSTSipA-C and ADF were labeled with Oregon green iodoacetamide and tetramethylrhodamine maleimide respectively (Molecular Probes) according to the manufacturer's instructions. Labeled proteins were separated from free fluorophore by gel filtration (Sephadex G-100; 10 mM Tris-Cl [pH 7.4], 150 mM NaCl, 0.2 mM DTT; Amersham). Protein-containing fractions were pooled and concentrated (Centricon 10; Millipore). Purified rabbit skeletal G-actin was labeled with tetramethylrhodamine iodoacetamide (TMR-IA, Molecular Probes) according to Theriot and Fung (1998).

Actin Comet Tail Motility Assay

Extract Preparation

Cytostatic factor-arrested *Xenopus laevis* egg extracts were prepared as described (Theriot et al., 1994). Extracts (~30 mg/ml^{-1}) were supplemented with 7.5 mM creatine phosphate, 1 mM ATP, 0.1 mM EGTA, 1 mM $MgCl_2$, and 100 mM sucrose, and aliquots were snap-frozen for storage.

PIP2 Vesicles

The lipid layer from *Xenopus* egg-crushing was retained (Theriot and Fung, 1998), resuspended in XB buffer (10 mM K-HEPES [pH 7.7], 100 mM KCl, 0.1 mM $CaCl_2$, 2 mM $MgCl_2$, 5 mM EGTA, 50 mM sucrose), and 50 nm diameter vesicles prepared by extrusion (LiposoFast, Glen Creston).

Bacterial Strains

pT7*icsA* encoding IcsA was generated by PCR from the *S. flexneri* virulence plasmid and cloning into pET3a (Novagen). pAT18 expressing *L. monocytogenes pprot-actA* and *L. innocua* rhamnose$^-$ CLIP 11262 are described by Kocks et al. (1995).

Cultured *E. coli* BL21 pT7*icsA* and *L. innocua* pAT18 resuspended in XB buffer were killed (chloramphenicol [40 μg/ml^{-1}], 0.02% [w/v] sodium azide) (20 min, RT). After centrifugation (8000 g, 5 min), pellets were washed and resuspended in fresh XB buffer to A_{600} = 5 (~4×10^9 bacteria ml^{-1}), then frozen at −80°C in 30% (v/v) glycerol.

Motility Assays

Xenopus extract (10 μl) with 0.5 μM Rh-ADF when appropriate was mixed with 0.1 vol bacteria or lipid vesicles and 0.05 vol Rh-actin (30 min, 4°C). Actin concentration was determined as ~7 μM (Loisel et al., 1999). XB buffer or 0.05–7 μM SipA, OG-labeled when appropriate, diluted in XB buffer, was added, and 1 μl was applied to a microscope slide and sealed with a coverslip. SipA was added after 30 min to allow comet tail assembly. Preparations were sealed (vaseline/lanolin/paraffin 1:1:1) and viewed by fluorescence microscopy (Leica DM IRBE). Digital images were captured (CCD camera, Hamamatsu) and analyzed (OpenLab, Improvision).

Actin Depolymerization

F-actin was preassembled by mixing purified rabbit skeletal muscle G-actin (2 μM) in G buffer (5 mM Tris-Cl [pH 8], 0.1 mM ATP, 0.2 mM $CaCl_2$, 0.02% NaN_3) with 0.02 vol 50× initiation buffer (100 mM $MgCl_2$, 50 mM ATP, 2.5 M KCl) and incubating (30 min, RT). Gelsolin-nucleated F-actin was prepared identically except G buffer contained 0.01 μM purified gelsolin (Cytoskeleton) and the mixture incubated longer (1 hr, RT).

Cosedimentation

Mixtures of SipA or GSTSipA-C and F-actin or gelsolin-nucleated F-actin (each 1 μM) were incubated (10 min, RT) in F buffer (10 mM Tris-Cl [pH 8], 0.1 M KCl, 0.1 mM ATP, 1 mM $MgCl_2$, 1 mM EGTA, 0.2 mM DTT). ADF/cofilin and/or DNase I (2 μM, Worthington) was then added (incubated 90 min, RT), and the mixture centrifuged (100,000 g, 25 min, 4°C). Supernatants and pellets were analyzed by SDS-PAGE.

Pyrene Assays

Pyrene-F-actin (1 μM, 10% pyrene-labeled) was incubated with SipA/GSTSipA-C (1 μM, 10 min, RT), then ADF/cofilin (4 μM), and pyrene fluorescence was monitored (LS50B fluorimeter, Perkin Elmer; excitation 365 nm, emission 395 nm).

Fluorescence Microscopy

Rh-F-actin (5 μM, 30% TMR-IA-labeled) was incubated with combinations of ADF/cofilin (8 μM) and SipA (5 or 1 μM) (2 min, RT). Aliquots were mounted in 0.5 vol ProLong Antifade reagent (Molecular Probes) and visualized by fluorescence microscopy (Leica DM IRBE).

Actin Binding

Proteins were dialyzed (10 mM PIPES [pH 6.6], 2 mM $MgCl_2$, 0.1 M KCl, 0.1 mM DTT) and clarified (100,000 g, 25 min). F-actin (2 μM) was incubated (20 min, RT) with ADF/cofilin, SipA, or in combination (2 μM) and centrifuged (100,000 g, 25 min, 4°C); supernatants and pellets were analyzed by SDS-PAGE.

Actin Severing

Cosedimentation

F-actin (2 μM), alone or premixed with SipA/GSTSipA-C (2 μM), was incubated with gelsolin (0.1–1 μM, Cytoskeleton) in F buffer (−EGTA,

+0.1 mM $CaCl_2$, 1 hr, RT) and centrifuged (100,000 g, 25 min, 4°C); supernatants and pellets were analyzed by SDS-PAGE.

Pyrene Assays

Pyrene-F-actin (2 μM) was incubated with SipA/GSTSipA-C (2 μM, 10 min, RT). Gelsolin (0.5 μM) was added, and pyrene fluorescence was monitored.

Fragment Annealing

F-actin (2 μM) was severed with gelsolin (0.5 μM, 1 hr, RT), and SipA added (2 μM, 1 hr, RT). Samples were centrifuged (100,000 g, 25 min, 4°C), and supernatants and pellets were analyzed by SDS-PAGE.

Transmission Electron Microscopy

F-actin (2 μM) was severed with gelsolin (0.5 μM, 1 hr, RT) and then centrifuged (100,000 g, 25 min, 4°C). SipA (2 μM) was added to the supernatant (1 hr, RT). Samples were negatively stained (2% [v/v] uranyl acetate) and examined as described (McGhie et al., 2001). Filament length was scored directly from TEM negatives.

Isothermal Titration Calorimetry

Isothermal titration calorimetry (ITC) was performed using a VP-ITC MicroCalorimeter (MicroCal). Five microliters SipA (45 μM) was injected every 4 min into 2 ml F-actin (5 μM) in F buffer until the titrant was in excess, and data were analyzed (Origin, MicroCal).

Acknowledgments

We thank Pascale Cossart for the gift of *Listeria* strains and Enrique Amaya for the gift of *Xenopus* eggs and assistance with extract preparation. We also thank Peter Hume and Colin Hughes for critical discussions. This work was supported by a Wellcome Trust Programme grant to V.K.

Received: September 26, 2003
Revised: December 12, 2003
Accepted: December 12, 2003
Published: February 26, 2004

References

Araya, E., Berthier, C., Kim, E., Yeung, T., Wang, X., and Helfman, D.M. (2002). Regulation of coiled-coil assembly in tropomyosins. J. Struct. Biol. *137*, 176–183.

Bamburg, J.R., McGough, A., and Ono, S. (1999). Putting a new twist on actin: ADF/cofilins modulate actin dynamics. Trends Cell Biol. *9*, 364–370.

Bernstein, B.W., and Bamburg, J.R. (1982). Tropomyosin binding to F-actin protects the F-actin from disassembly by brain actin-depolymerising factor. Cell Motil. *2*, 1–8.

Burtnick, L.D., Koepf, E.K., Grimes, J., Jones, E.Y., Stuart, D.I., McLaughlin, P.J., and Robinson, R.C. (1997). The crystal structure of plasma gelsolin: implications for actin severing, capping and nucleation. Cell *90*, 661–670.

Carlier, M.F., Laurent, V., Santolini, J., Melki, R., Didry, D., Xia, G.X., Hong, Y., Chua, N.H., and Pantaloni, D. (1997). Actin depolymerising factor (ADF/cofilin) enhances the rate of filament turnover: implication in actin based motility. J. Cell Biol. *136*, 1307–1322.

Chen, L.-M., Hobbie, S., and Galán, J.E. (1996). Requirement of CDC42 for *Salmonella*-induced cytoskeletal and nuclear responses. Science *274*, 2115–2118.

Cooper, J.A. (2002). Actin dynamics: tropomyosin provides stability. Curr. Biol. *12*, R523–R525.

David, V., Gouin, E., Troys, M.V., Grogan, A., Segal, A.W., Ampe, C., and Cossart, P. (1998). Identification of cofilin, coronin, Rac and CapZ in actin tails using a *Listeria* affinity approach. J. Cell Sci. *111*, 2877–2884.

DesMarais, V., Ichetovkin, I., Condeelis, J., and Hitchcock-DeGregori, S.E. (2002). Spatial regulation of actin dynamics: a tropomyosin-free, actin-rich compartment at the leading edge. J. Cell Sci. *115*, 4649–4660.

Egile, C., Loisel, T.P., Laurent, V., Li, R., Pantaloni, D., Sansonetti, P.J., and Carlier, M.-F. (1999). Activation of the Cdc42 effector N-WASP by the *S. flexneri* IcsA protein promotes actin nucleation by the Arp2/3 complex and bacterial actin-based motility. J. Cell Biol. *146*, 1319–1332.

Finlay, B.B., and Falkow, S. (1997). Common themes in microbial pathogenicity revisited. Microbiol. Mol. Biol. Rev. *61*, 136–169.

Finlay, B.B., Ruschkowski, S., and Dedhar, S. (1991). Cytoskeletal rearrangements accompanying *Salmonella* entry into epithelial cells. J. Cell Sci. *99*, 283–296.

Frischknecht, F., and Way, M. (2001). Surfing pathogens and the lessons learned for actin polymerisation. Trends Cell Biol. *11*, 30–37.

Galán, J.E., and Zhou, D. (2000). Striking a balance: modulation of the actin cytoskeleton by *Salmonella*. Proc. Natl. Acad. Sci. USA *97*, 8754–8761.

Galkin, V.E., Orlova, A., VanLoock, M.S., Zhou, D., Galán, J.E., and Egelman, E.H. (2002). The bacterial protein SipA polymerises G-actin and mimics muscle nebulin. Nat. Struct. Biol. *9*, 518–521.

Gruenheid, S., and Finlay, B.B. (2003). Microbial pathogenesis and cytoskeletal function. Nature *422*, 775–781.

Hayward, R.D., and Koronakis, V. (1999). Direct nucleation and bundling of actin by the SipC protein of invasive *Salmonella*. EMBO J. *18*, 4926–4934.

Hayward, R.D., and Koronakis, V. (2002). Direct modulation of the host cell cytoskeleton by *Salmonella* actin-binding proteins. Trends Cell Biol. *12*, 15–20.

Higashide, W., Dai, S., Hombs, V.P., and Zhou, D. (2002). Involvement of SipA in modulating actin dynamics during *Salmonella* invasion into cultured epithelial cells. Cell. Microbiol. *4*, 357–365.

Hitchcock, S.E., Carlsson, L., and Lindberg, U. (1976). Depolymerisation of F-actin by deoxyribonuclease I. Cell *7*, 531–542.

Kaniga, K., Tucker, S., Trollinger, D., and Galán, J.E. (1995). Homologs of the *Shigella* IpaB and IpaC invasins are required for *S. typhimurium* entry into cultured epithelial cells. J. Bacteriol. *177*, 3965–3971.

Kinosian, H.J., Selden, L.A., Estes, J.E., and Gershman, L.C. (1996). Kinetics of gelsolin interaction with phalloidin-stabilised F-actin. Rate constants for binding and severing. Biochemistry *35*, 16550–16556.

Kocks, C., Marchand, J.-B., Gouin, E., d'Hauteville, H., Sansonetti, P.J., Carlier, M.-F., and Cossart, P. (1995). The unrelated surface proteins ActA of *L. monocytogenes* and IcsA of *S. flexneri* are sufficient to confer actin-based motility on *L. innocua* and *E. coli* respectively. Mol. Microbiol. *18*, 413–423.

Kubori, T., and Galán, J.E. (2003). Temporal regulation of *Salmonella* virulence effector function by proteosome-dependent protein degradation. Cell *115*, 333–342.

Kwiatkowski, D.J. (1999). Function of gelsolin: motility, signalling, apoptosis, cancer. Curr. Opin. Cell Biol. *11*, 103–108.

Laine, R.O., Phaneuf, K.L., Cunningham, C.C., Kwiatkowski, D., Azuma, T., and Southwick, F.S. (1998). Gelsolin, a protein that caps barbed ends and severs actin filaments, enhances the actin-based motility of *L. monocytogenes* in host cells. Infect. Immun. *66*, 3775–3782.

Leonard, S.A., Giltis, A.G., Petrella, E.C., Pollard, T.D., and Lattman, E.E. (1997). Crystal structure of the actin-binding protein actophorin from *Acanthamoeba*. Nat. Struct. Biol. *4*, 369–373.

Lesser, C.F., and Miller, S.I. (2001). Expression of microbial virulence proteins in *S. cerevisiae* models mammalian infection. EMBO J. *20*, 1840–1849.

Lilic, M., Galkin, V.E., Orlova, A., Van Loock, M.S., Egelman, E.H., and Stebbins, C.E. (2003). *Salmonella* SipA polymerises actin by stapling filaments with nonglobular protein arms. Science *301*, 1918–1921.

Loisel, T.P., Boujemaa, R., Pantaloni, D., and Carlier, M.-F. (1999). Reconstitution of actin-based motility of *Listeria* and *Shigella* using pure proteins. Nature *401*, 613–616.

Lu, M., Witke, W., Kwiatkowski, D.J., and Kosik, K.S. (1997). Delayed retraction of filopodia in gelsolin null mice. J. Cell Biol. *138*, 1279–1287.

Ma, L., Cantley, L.C., Janmey, P.A., and Kirschner, M.W. (1998). Corequirement of specific phosphoinositides and small GTP-binding protein Cdc42 in inducing actin assembly in *Xenopus* egg extracts. J. Cell Biol. *140*, 1125–1136.

Machesky, L.M., and Insall, R.H. (1998). Scar1 and the related Wiskott-Aldrich syndrome protein, WASP, regulate the actin cytoskeleton through the Arp2/3 complex. Curr. Biol. *8*, 1347–1356.

McGhie, E.J., Hayward, R.D., and Koronakis, V. (2001). Co-operation between actin-binding proteins of invasive *Salmonella*: SipA potentiates SipC nucleation and bundling of actin. EMBO J. *20*, 2131–2139.

McGough, A., Pope, B., Chiu, W., and Weeds, A. (1997). Cofilin changes the twist of F-actin: implications for actin filament dynamics and cellular function. J. Cell Biol. *138*, 771–781.

McLaughlin, P.J., Gooch, J.T., Mannherz, H.G., and Weeds, A.G. (1993). Structure of gelsolin segment 1-actin complex and the mechanism of filament severing. Nature *364*, 685–692.

Mitra, K., Zhou, D., and Galán, J.E. (2000). Biophysical characterisation of SipA, an actin-binding protein from *S. enterica*. FEBS Lett. *482*, 81–84.

Moriyama, K., and Yahara, I. (1999). Two activities of cofilin, severing and accelerating directional depolymerisation of actin filaments, are affected differentially by mutations around the actin-binding helix. EMBO J. *18*, 6752–6761.

Nyåkern-Meazza, M., Narayan, K., Schutt, C.E., and Lindberg, U. (2002). Tropomyosin and gelsolin cooperate in controlling the microfilament system. J. Biol. Chem. *277*, 28774–28779.

Ono, S., and Ono, K. (2002). Tropomyosin inhibits ADF/cofilin-dependent actin filament dynamics. J. Cell Biol. *156*, 1065–1076.

Pantaloni, D., LeClainche, C., and Carlier, M.-F. (2001). Mechanism of actin-based motility. Science *292*, 1502–1506.

Pollard, T.D., and Borisy, G.G. (2003). Cellular motility driven by assembly and disassembly of actin filaments. Cell *112*, 453–465.

Pope, B.J., Gonsior, S.M., Yeoh, S., McGough, A., and Weeds, A.G. (2000). Uncoupling actin filament fragmentation by cofilin from increased subunit turnover. J. Mol. Biol. *298*, 649–661.

Renoult, C., Ternent, D., Maciver, S.K., Fattoum, A., Astier, C., Benyamin, Y., and Roustau, C. (1999). The identification of a second cofilin binding site on actin suggests a novel, intercalated arrangement of F-actin binding. J. Biol. Chem. *274*, 28893–28899.

Rosenblatt, J., Agnew, B.J., Abe, H., Bamburg, J.R., and Mitchison, T.J. (1997). *Xenopus* actin depolymerising factor/cofilin (XAC) is responsible for the turnover of actin filaments in *L. monocytogenes* tails. J. Cell Biol. *136*, 1323–1332.

Scherer, C.A., Cooper, E., and Miller, S.I. (2000). The *Salmonella* type III secretion translocon protein SspC is inserted into the epithelial plasma membrane upon infection. Mol. Microbiol. *37*, 1133–1145.

Sheterline, P., Clayton, J., and Sparrow, J.C. (1998). Actin, Fourth Edition (Oxford: Oxford University Press).

Stebbins, C.E., and Galán, J.E. (2001). Structural mimicry in bacterial virulence. Nature *414*, 77–81.

Studier, W., and Moffat, B.A. (1986). Use of bacteriophage T7 RNA polymerase to direct selective high level expression of cloned genes. J. Mol. Biol. *189*, 113–130.

Theriot, J.A., and Fung, D.C. (1998). *L. monocytogenes*-based assays for actin assembly factors. Methods Enzymol. *298*, 114–122.

Theriot, J.A., Rosenblatt, J., Portnoy, D.A., Goldschmidt-Clermont, P.J., and Mitchinson, T.J. (1994). Involvement of profilin in the actin-based motility of *L. monocytogenes* in cells and cell-free extracts. Cell *76*, 505–517.

Waterman, S.R., and Holden, D.W. (2003). Functions and effectors of the *Salmonella* pathogenicity island 2 type III secretion system. Cell. Microbiol. *5*, 501–511.

Wegner, A. (1982). Kinetic analysis of actin assembly suggests that tropomyosin inhibits spontaneous fragmentation of actin filaments. J. Mol. Biol. *161*, 217–227.

Welch, M.D., Rosenblatt, J., Skoble, J., Portnoy, D.A., and Mitchison, T.J. (1998). Interaction of human Arp2/3 complex and the *L. monocytogenes* ActA protein in actin filament nucleation. Science *281*, 105–108.

Xu, J., Casella, J.F., and Pollard, T.D. (1999). Effect of capping protein, CapZ, on the length of actin filaments and mechanical properties of actin filament networks. Cell Motil. Cytoskeleton *42*, 73–81.

Yamaguchi, S., Fujita, H., Sugata, K., Taira, T., and Iino, T. (1984). Genetic analysis of H2, the structural gene for phase-2 flagellin in *Salmonella*. J. Gen. Microbiol. *130*, 255–265.

Yeoh, S., Pope, B., Mannherz, H.G., and Weeds, A. (2002). Determining the differences in actin binding by human ADF and cofilin. J. Mol. Biol. *315*, 911–925.

Zhou, D., Mooseker, M.S., and Galán, J.E. (1999a). Role of the *S. typhimurium* actin-binding protein SipA in bacterial internalisation. Science *283*, 2092–2095.

Zhou, D., Mooseker, M.S., and Galán, J.E. (1999b). An invasion-associated *Salmonella* protein modulates the actin-binding activity of plastin. Proc. Natl. Acad. Sci. USA *96*, 10176–10181.